

# Characterization of VUV4 SiPM for Liquid Argon detector

L. Wang<sup>a</sup>, M.Y. Guan<sup>a,b,c</sup>, H.J. Qin<sup>d</sup>, C. Guo<sup>a,b,c\*</sup>, X.L. Sun<sup>a,b,c†</sup>,  
C.G. Yang<sup>a,b,c</sup>, Q. Zhao<sup>b,c</sup>, J.C. Liu<sup>b,c</sup>, P. Zhang<sup>a,b,c</sup>, Y.P. Zhang<sup>a,b,c</sup>,  
W.X. Xiong<sup>b,c</sup>, Y.T. Wei<sup>b,c</sup>, Y.Y. Gan<sup>b,c</sup>, J.J. Li<sup>e</sup>,

<sup>a</sup> *State Key Laboratory of Particle Detection and Electronics, Beijing, China*

<sup>b</sup> *Experimental Physics Division, Institute of High Energy Physics, Beijing, China*

<sup>c</sup> *School of Physics, University of Chinese Academy of Science, Beijing, China*

<sup>d</sup> *School of Internet of Things Engineering, JiangNan University, Wuxi, China*

<sup>e</sup> *School of Nuclear Science and Engineering, North China Electric Power University, Beijing, China*

---

## Abstract

Particle detectors based on liquid argon have recently become recognised as an extremely attractive technology for the direct detection of dark matter and the measurement of coherent elastic neutrino-nucleus scattering. A program using a dual-phase liquid argon detector with a fiducial mass of 200 kg to detect coherent elastic neutrino-nucleus scattering at Taishan Nuclear Power Plant has been proposed. SiPM will be used in this detector as the photon sensor because of its high radio-purity and high photon detection efficiency. S13370-6050CN SiPM, made by Hamamatsu, is expected to be functional well in liquid argon thus is a good choice for the detector. In this paper, the characterisation of S13370-6050CN SiPM, including the cross talk and after pulse probabilities at liquid argon temperature, was studied. Besides, the temperature dependence of break down voltage, dark count rate and relative quantum efficiency were presented as well.

*Keywords:* Coherent Elastic Neutrino-nucleus Scattering, Liquid Argon, SiPM

---

\*Corresponding author. Tel: +86-01088236256. E-mail address: guocong@ihep.ac.cn (C. Guo).

†Corresponding author. Tel: +86-01088236069. E-mail address: sunxl@ihep.ac.cn (X.L. sun)

---

## 1. Introduction

Coherent elastic neutrino-nucleus scattering ( $\text{CE}\nu\text{NS}$ ), which was first theorised by Freedman in 1974 [1], is the dominated interaction for neutrinos with the energy less than 100 MeV. The COHERENT collaboration achieved the first measurement of  $\text{CE}\nu\text{NS}$  by using 14.6 kg CsI(Na) crystal detector to detect the neutrinos from the spallation neutron source at Oak Ridge National Laboratory (ORNL) in 2017 [2]. Recently, they reported the first detection of  $\text{CE}\nu\text{NS}$  on argon using the CENNS-10 liquid argon detector [3]. A dual-phase liquid argon time projection chamber (TPC) with 200 kg fiducial mass was proposed to measure  $\bar{\nu}_e$ -Ar  $\text{CE}\nu\text{NS}$  process [4]. The detector is expected to be adjacent to the JUNO-TAO experiment [5], which is about 35 m from a reactor core with 4.6 GW thermal power at Taishan. Since the signal is concentrated in the sub-keV region and the event rate is very low, single photon detection ability and high detector radio-purity, including the target and detector components, become the basic requirements of the detector.

Silicon photo-multipliers (SiPM), which were originally developed in Russia in the mid-1980s [6], have known as a fast development in the past few years as a possible replacement for conventional photo-multiplier tubes (PMT). Compared with PMTs, SiPM has lower radioactive background and higher photon quantum efficiency, which make them the most appealing photon sensor for liquid argon detector. However, the gain of SiPM is usually  $\sim 10^6$ . Thus, a preamplifier is necessary to realize single photon signal detection. The liquid argon detector is operated at 87K, where most of SiPMs or amplifiers can not work properly [7]. Therefore, a set of SiPM and preamplifier working well at 87K is urgent relevance.

The S13770-6050CN [8] SiPM reported in this paper is a Vacuum Ultra-Violet sensitive SiPM developed by Hamamatsu specially for cryogenic experiments. Here, its performance at  $\sim 87\text{K}$  was studied in detail. The results proved able to achieve the functionality combining with our electronics. Besides, some significant parameters of the S13770-6050CN SiPM, such as dark count rate and break down voltage from 87K up to room temperature, are recorded in this paper.

## 2. Experimental Setup

The cryogenic system is shown in Fig. 1. A 6 mm\*6 mm SiPM chip is placed in a stainless steel (SST) chamber which is put in a dewar. A liquid nitrogen tank is standing on the ground nearby for cooling the system by a copper hose connecting. Two Pt100 sensors have been used in this system. One is put inside the SST chamber to monitor the temperature of the SiPM in real time, and the other is located in the interlayer between the dewar and the SST chamber to serve as the input of the temperature control system. It controls the injection of liquid nitrogen by adjusting the switch of the electromagnetic valve, so as to control the temperature of the system. The accuracy of the temperature control system is within  $\pm 1$  K and the detail can be found in Ref [9]. An LED with a peaked wavelength of 425 nm is placed in the top of the SST chamber to be used as a light source. A silicon photocell (model LONGXINDA LXD44MQ) is placed next to the LED to monitor its stability [10]. The LED is driven by a pulse generator (Tektronix, AFG31102, 100M, 2CH). During the whole experiment, the LED and the silicon photocell rest at room temperature. Before sent into the oscilloscope (LeCroy 610Zi, 250MHz sampling frequency) for pulses recording, signals from the SiPM are amplified by a LMH6629 preamplifier which worked at the same temperature as the SiPM. On the other hand, signals from the silicon photocell are amplified by a warm amplifier (model AD825 LF353). Two RAGOL DP831A DC power supplies support  $\pm 5$  V voltage to two amplifiers separately and a DH 1765-4 DC power supply serves as the bias source of the SiPM.

Four different kinds of DAQ setups have been used in the measurement.

(A) While measuring the break down voltage ( $V_{bd}$ ), the LED is driven by the pulse generator with a periodic square pulses of 1 kHz and the oscilloscope is triggered by synchronous pluses. Signals of the LED tigger and SiPM are recorded and the time window is set to 500 ns.

(B) While measuring the relative quantum efficiency (QE), the setups are basically same as case A except that the time window is set to 5  $\mu$ s and signals from the silicon photocell are also recorded.

(C) While measuring the correlated signal probabilities, the LED is off. Only the SiPM signals are recorded and the oscilloscope is at self-trigger mode. The time window is set to 500  $\mu$ s because we aim to analyse the correlated signals which follow behind the primitive pulses.

(D) While measuring the dark counting rate, the signals are directly sent

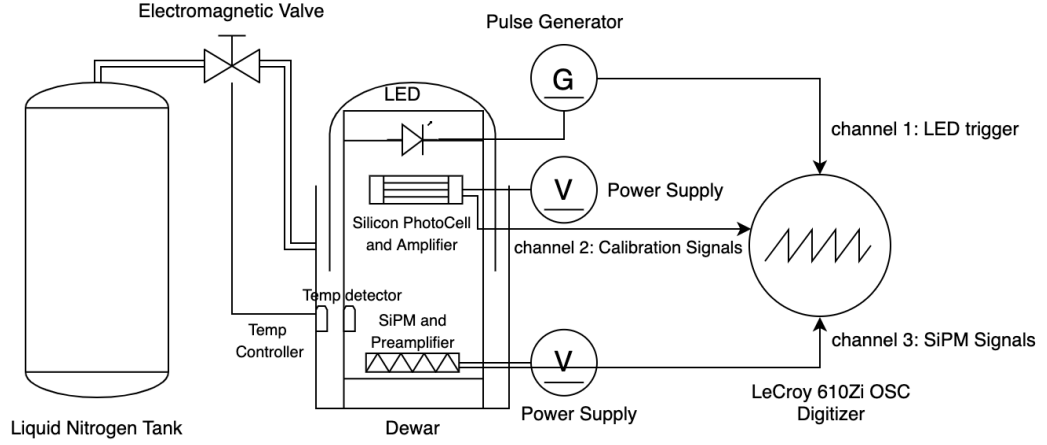


Figure 1: Scheme of the cryogenic system.

to a LTD (CAEN, N844). The output of the LTD is sent to a scaler (CAEN, N145 ) for counting.

All the signals are recorded by the oscilloscope and the data sampling rate is set to 500 MS/s.

LMH6629 is a high-speed, ultra-low noise amplifier designed for the applications requiring wide bandwidth with high gain and low noise [11]. Although the official claims that its working temperature is 233 K to 398 K, the application reported in Ref. [12] shows that the amplifier can even work at 60 K. Therefore, in this work, LMH6629 is chosen to amplify the signals from the SiPM. The circuit diagram, which inherits from Ref. [12], is shown in Fig. 2 and the values of the components used in this work is presented in Tab. 1.

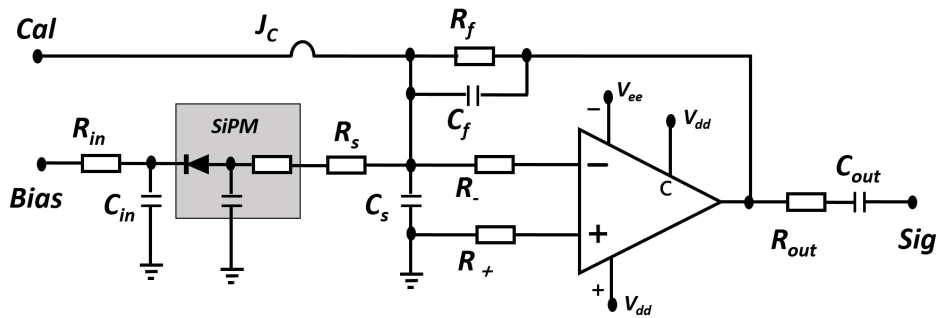


Figure 2: Circuit diagram of the readout.

Table 1: The values of the components shown in fig. 2 used in this work.

Resistance	$R_{in}$	$R_s$	$R_f$	$R_{out}$	$R_-$	$R_+$
Value	10 k $\Omega$	10 $\Omega$	2 k $\Omega$	50 $\Omega$	2 k $\Omega$	5 $\Omega$
capacitance	$C_{in}$	$C_s$	$C_f$	$C_{out}$		
Value	100 nf	30 nf	10 nf	10 nf		

### 3. Stability test of LMH6629

The tests reported in Ref. [12] show that the amplifier LMH6629 can still work when the temperature is down to 60 K, but its cryogenic performance, especially the gain stability around 87 K, is not clear yet. Thus, before the characterisation measurements of the SiPM, the linearity of LMH6629 amplifier need to be estimated, to guarantee the linearity of the SiPM outputs.

The circuit diagram shown in Fig. 2 is used in this measurement, but the SiPM is removed and  $J_c$  is connected. The input signal, which is a periodic square pulse with a frequency of 1 kHz, is generated by the pulse generator mentioned in Sec. 2. The width of the input pulse is 100 ns and the amplitude is 2 mV. The two signals generated by the pulse generator are identical and synchronised, one is directly sent to the oscilloscope for pulses recording, while the other is amplified before sent to the oscilloscope. The charge ratio of the two signals received by the oscilloscope is used to calculate the gain of the amplifier. Fig. 3 shows the gain variation along with temperature and the stability is within 2%.

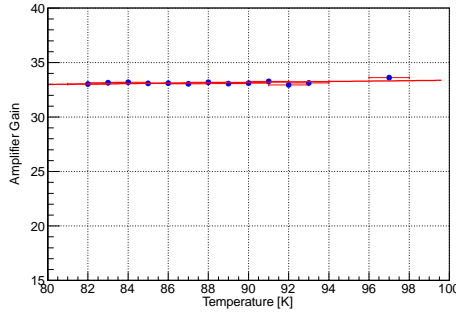


Figure 3: Gain of the amplifier vs temperature. Gain is calculate by the charge ratio of signals before and after amplification. The errors of the X-axis are the accuracy of the temperature control system and the errors of the Y-axis are statistical only.

Except the temperature fluctuation during the experiment, the input charge will also change due to different number of SiPM cells fire. According to Ref. [8], the typical gain of S13370-6050CN SiPM is  $5.8 \times 10^6$ , thus one photoelectron (P.E.) corresponds to a charge of  $\sim 0.9$  pC. In the test of gain variation along with the input charge, the width of the input pulse is set to 100 ns which is the typical width of the SiPM output signals, while the amplitude changes from 2 mV to 15 mV which is equivalent to the input charge from 0.5 pC to 7.5 pC. The result is shown in Fig. 4 and the variation is within 3%.

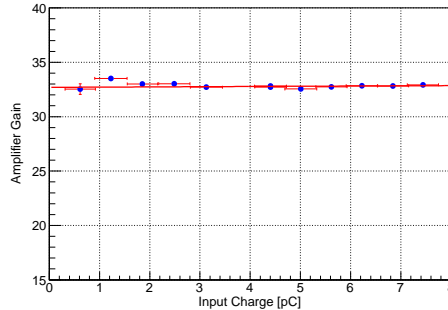


Figure 4: Gain of the amplifier vs input charge. Gain is calculate by the charge ratio of signals before and after amplification. The errors of the X-axis are the accuracy of the temperature control system and the errors of the Y-axis are statistical only.

## 4. Data Analysis

### 4.1. Signal composition

A custom data analysis program has been developed and a detailed analysis has been performed. For each event, the program calculates the peak amplitude and the pulse charge. For simplicity, the amplitude of single photoelectron (SPE) is defined as 1 P.E.A. and the charge of single photoelectron is defined as 1 P.E.C.. An example of a scatter distribution of charge and amplitude is shown in Fig. 5 of which the SiPM is operated at 87 K with 3 V over voltage. The events shown in Fig. 5 consist of the following four parts [13–15]:

A. Dark noise : In the absence of light, dark noise, which is produced by carriers generated in the depletion region, constitutes the main part of the signal. The dark noise is the SPE event thus has an amplitude centred at

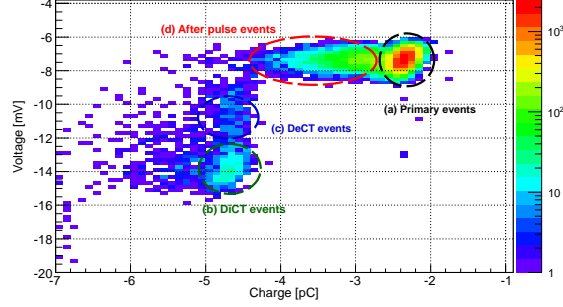


Figure 5: Scatter distribution of charge VS amplitude of S13370-6050CN SiPM operated at 87 K with an over voltage of 3 V. Events in the black circle are dark noises, in the red circle are after pulses, in the blue circle are delayed crosstalks and in the green circle are direct crosstalks.

1 P.E.A. and a charge centred at 1 P.E.C.. A sample pulse of dark noise is shown in Fig. 6-(a).

B. Direct crosstalk: Direct crosstalk (DiCT) is caused by a photon which is emitted by the movement of accelerated carriers in the strong field during the primary avalanche triggering a neighbouring pixel within an extremely short time interval. Thus, a DiCT signal has an amplitude centred at 2 P.E.A. and a charge centred at 2 P.E.C., which is just similar to a 2 P.E. event. A sample pulse of DiCT is shown in Fig. 6-(b).

C. Delayed crosstalk: Delayed crosstalk (DeCT) occurs when the photons produced in the primary avalanche absorbed in the non-depleted region of a neighbouring cell. Before triggering a second avalanche, the carriers have to diffuse into the high-field region, thus the time difference between the two avalanches is around several nanosecond. Based on its mechanism, the amplitude of DeCT should be between 1 P.E.A. to 2 P.E.A. while the charge should be centred at 2 P.E.C.. The example pulse of DeCT is shown in Fig. 6-(c).

D. After pulse: After pulse (AP) is observed when a secondary electron is trapped by some sort of impurity during the primary avalanche. The trapped electron is then released after a characteristic time from nanosecond to microsecond and finally results a second avalanche. In principle, the time interval and energy distribution depend on the location of trapped electron. The AP event should have an amplitude around 1 P.E.A. while its charge should be between 1 P.E.C. to 2 P.E.C. because the second avalanche dis-

charge starts in the middle. The example pulse of AP is shown in Fig. 6-(d).

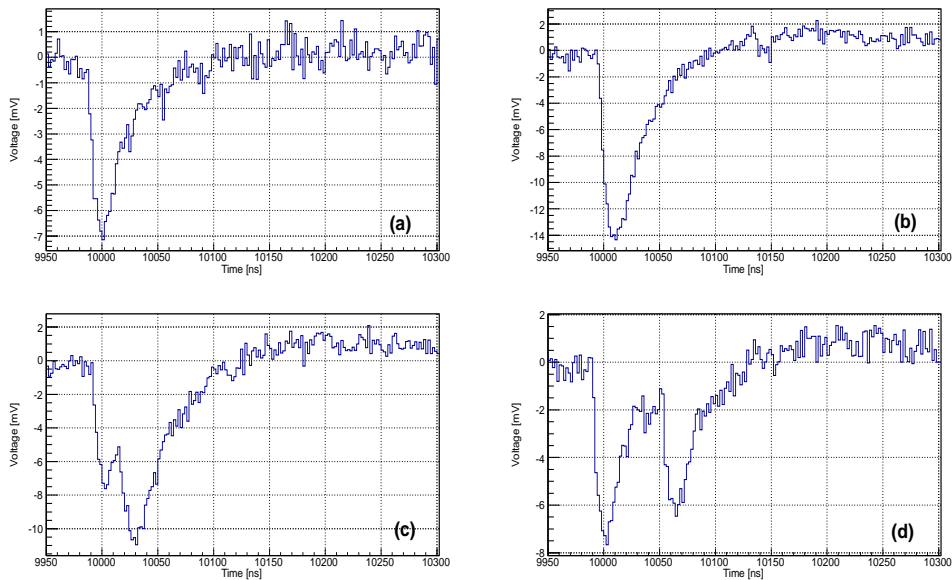


Figure 6: Example pulses for different events.

#### 4.2. Pulse fitting

As described in Sec. 4.1, different kinds of signals can be identified with the charge and amplitude information. In order for better understanding of the energy and time information of DeCT and AP events, a program for pulse fitting has been developed.

As can be seen from Fig. 6, the delayed pulse overlaps on the primary SPE pulse, thus the whole pulse can be described by Eq. 1, which is a superposition of two Landau Distributions [16] with seven parameters.

$$Fit(x) = A_1 Landau(x, p_1, w_1) + A_2 Landau(x, p_2, w_2) + BL \quad (1)$$

where  $A_1$  and  $A_2$  are amplitudes of two Landau distributions,  $p_1$ ,  $p_2$  and  $w_1$ ,  $w_2$  are the locations of peaks and the widths of waveforms separately,  $BL$  is the baseline of signals. The first term of Eq. 1 is for describing the primary pulse and the second term is for the delayed pulse. Fig. 7 shows an example of the fitting result.

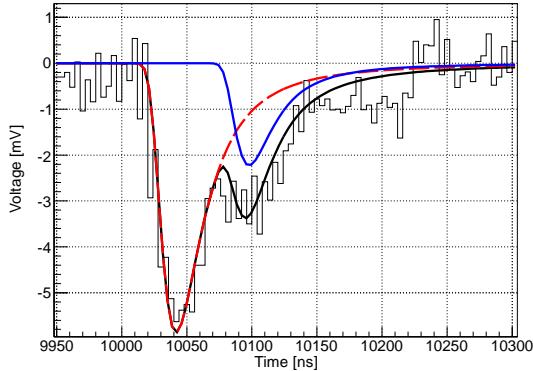


Figure 7: A sample of AP event fitted according to Eq. 1. The black curve is the fitted raw waveform, the red dashed curve is the primary pulse, the blue curve is the after pulse.

## 5. Results

The main purpose of this work is to study the application prospect of S13370-6050CN SiPM in liquid argon detectors. According to Ref. [17], the SiPM used in a two-phase liquid argon detector needs to meet at least the following two points:

A. The dark count rate (DCR) should be less than  $0.1 \text{ Hz/mm}^2$  to keep pulse shape discrimination effective;

B. The total correlated noise probability, namely the sum of DiCT, DeCT and AP, should be less than 60% for energy reconstruction of S2 signal.

The DCR and total correlated noise probability changes along with the over voltage ( $V_{over}$ ), which is the difference between the supplying bias and the breakdown voltage, therefore the break down voltage must be accurately measured.

### 5.1. Breakdown voltage

The breakdown voltage ( $V_{bd}$ ) is the bias point at which the electric field strength generated in the depletion region is just sufficient to create Geiger discharge. In principle,  $V_{bd}$  is the voltage where the gain of the SiPM, which is defined as Eq. 2, drops to exactly zero, thus  $V_{bd}$  can be calculated as the intersection of linear fits which is presented in Fig. 8. Fig. 9 shows the function of  $V_{bd}$  along with temperature. Above 120 K,  $V_{bd}$  decreases linearly with temperature, which is about  $0.5 \text{ V}/10 \text{ K}$ , while below 120 K the decrease tends to be slow.

$$G = \frac{Q}{q_e} = \frac{\int I(t)dt}{q_e} = \frac{\int V_{out}dt}{R_{load}G_{Amp}q_e} \quad (2)$$

where  $G$  is the gain of the SiPM,  $Q$  is the charge of one avalanche,  $q_e$  is the charge of an electron,  $I$  is the current,  $V_{out}$  is the output amplitude of the signal,  $R_{load}$  is the matching resistance, which is  $50 \Omega$ ,  $G_{Amp}$  is the gain of the preamplifier.

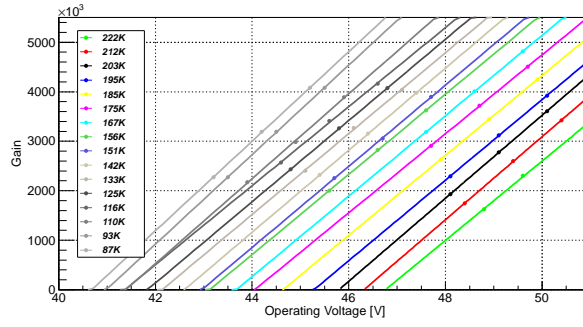


Figure 8: Charge vs  $V_{bd}$  at different temperature.

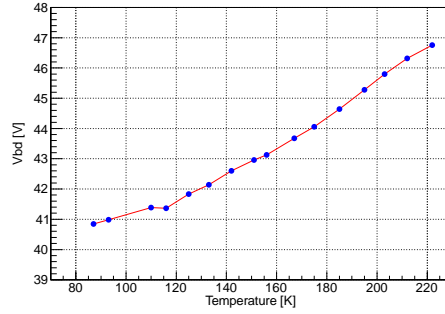


Figure 9: Change of  $V_{bd}$  along with temperature, the errors in the X-axis are the accuracy of the temperature system, which is  $\pm 1$  K, the errors in the Y-axis are statistical only.

### 5.2. Dark counting rate

The event rate of dark noises is called dark counting rate (DCR), which is caused by thermally generated electrons that trigger an avalanche in active volumes. The DCR can be measured with a counting system with a threshold

of 0.5 P.E. level. The change of DCR with threshold is shown in Fig. 10 and the event rates at 0.5 P.E., 1.5 P.E., and 2.5 P.E. are indicated in the plot by the vertical dotted lines.

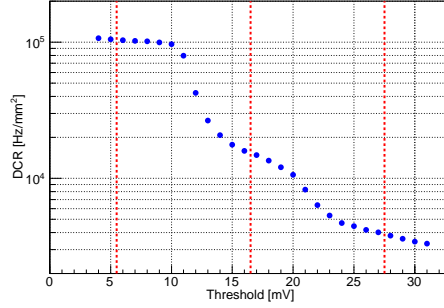


Figure 10: DCR of the SiPM operated at  $V_{over}=4$  V at 298 K as a function of the discriminator threshold. The locations of 0.5 P.E., 1.5 P.E., and 2.5 P.E. are indicated in the plot by vertical dotted lines separately.

As discussed in Ref. [13–15], DCR is the function of temperature and  $V_{over}$  and our measurement results are shown in Fig. 11. The DCR is  $\sim 0.003$  Hz for the tested SiPM at 87 K with an over voltage of 4 V.

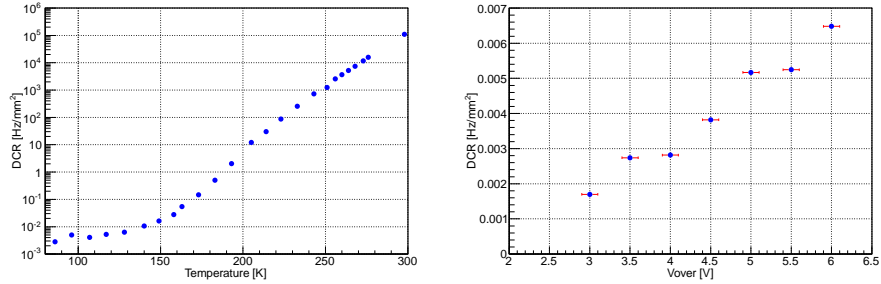


Figure 11: Left: Change of DCR along with temperature,  $V_{over}$  is set to 4 V during the test. Right: Change of DCR along with  $V_{over}$  at 87 K, the errors shown in the X-axis are caused by the temperature variation, which is  $\pm 1$  K, during the test.

### 5.3. Correlated signals

Correlated signals are the general term of DiCT, DeCT and AP and the definition and characteristics are introduced in Sec. 4.1. Fig. 12 shows the tendency of the probabilities of DiCT, DeCT and AP. At 87K, The total

correlated signal probability is  $\sim 14\%$  at  $V_{over} = 4$  V, which could satisfy the requirements of using SiPM in liquid argon proposed by DarkSide [17].

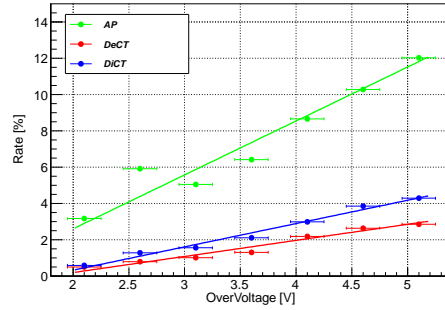


Figure 12: The changes of the probabilities of DiCT, DeCT and AP along with  $V_{over}$ . The errors in the X-axis are caused by the temperature variation.

In order to study the time and energy characterisation of different kinds of the correlated signals, a program based on pulse fitting has been developed, which has been discussed in Sec. 4.2. The time interval distribution between correlated pulses (DeCT and AP) and the primary DCR is shown in Fig. 13. The X-axis is the time difference of the delayed pulse and the primary pulse, which is calculated as  $p_2 - p_1$  of Eq. 1. Oppositely, the Y-axis is the charge of the delayed pulse, which is the integral of the blue line shown in Fig. 7. The figure shows there is a direct proportion between the delay time and pulse energy for AP events, which possibly indicates that the further the electron is trapped from anode (higher energy), the faster the electron is released from the impurity (less time interval).

#### 5.4. Relative quantum efficiency

One of the advantages of S13370-6050CN SiPM is that it can directly detect the photons emitted by liquid argon, of which the wavelength is peaked at 128 nm. But the official also claims that it has the largest quantum efficiency at  $\sim 500$  nm [8]. For liquid argon detector [18, 19], nearly all the detectors prefer not to read the 128 nm directly, one reason is that the photon sensors have very low quantum efficiency at 128 nm and another reason is that the wavelength shifter, 1,1,4, 4-tetraphenyl-1,3-butadiene (TPB) [20], has more than 100% photon conversion efficiency [21], which means that more than one 420 nm photons will be emitted when one 128 nm photon is absorbed. The DarkSide collaboration will continue to use the wavelength

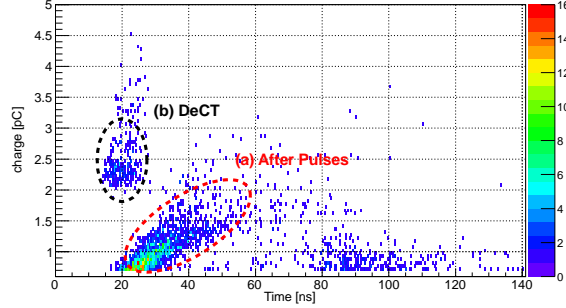


Figure 13: The time difference between correlated signals and primary DCR VS the energy of the correlated signals. X-axis the time difference for the delayed pulse and the primary pulse, Y-axis is the charge of the delayed pulse. Events in the red circle are AP and in the black circle are DeCT. The events in the time range of 80-100 ns with charge less than 1 pC are due to the failure of fitting, which are actually normal DCR events with a little larger baseline jitter.

shift scheme in DS-20k experiment [17]. In Ref. [8], the quantum efficiency is measured at 298 K, while according to Ref. [22], the quantum may be very different at room temperature and liquid argon temperature. In this work, a 425 nm LED is used to study the relative quantum efficiency and Fig. 14 shows the result which indicates that the quantum efficiency difference of S13370-6050CN SiPM for 300 K and 87 K is  $\sim 10\%$ .

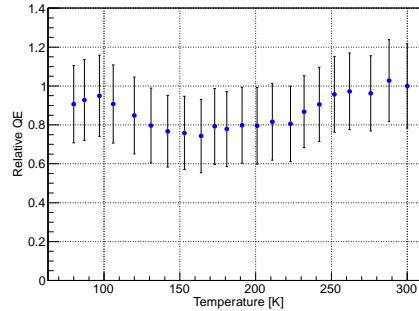


Figure 14: The relative quantum efficiency at different temperature. The results are normalised to the point of 300K and the errors shown in the Y-axis are statistical only.

## 6. Summary

A program of using liquid argon to detect  $\bar{\nu}_e$ -Ar CE $\nu$ NS at Taishan Nuclear Power Plant has been proposed and SiPM will be used as the photon sensors. In order to test the application prospect of SiPM in liquid argon, a cryogenic system has been developed and S13370-6050CN SiPM has been tested in detail. The DCR is below 0.003 Hz/mm<sup>2</sup> and the total correlated noise is less than 14% at 87K with 3 V over voltage. Our results indicate that the S13370-6050CN SiPM made by Hamamatsu is a good candidate for liquid argon detector.

## 7. Acknowledgements

This work is supported by National Key R&D Program of China (Grant No. 2016YFA0400304) and National Natural Science Foundation of China (Grant No. 12020101004).

The authors would like to thank Alessandro Razeto, Paolo Musico and Gemma Testera of INFN for their help during the design of the readout system.

## References

### References

- [1] D.Z. Freedman, Coherent effects of a weak neutral current, Phys. Rev. D 9, 1389 (1974).
- [2] COHERENT collaboration, Observation of Coherent Elastic Neutrino-Nucleus Scattering, Science 357, 1123-1126 (2017).
- [3] COHERENT collaboration, First Detection of Coherent Elastic Neutrino-Nucleus Scattering on Argon, arXiv:2003.10630v6.
- [4] Yu-Ting Wei, Meng-Yun Guan, Jin-Chang Liu, Ze-Yuan Yu, Chang-Gen Yang, Cong Guo, Wei-Xing Xiong, You-Yu Gan, Qin Zhao, Jia-Jun Li, Prospects of detecting the reactor  $\bar{\nu}_e$ -Ar coherent elastic scattering with a low threshold dual-phase argon time projection chamber at Taishan, arXiv:2012.00966v3.

- [5] JUNO collaboration, TAO Conceptual Design Report: A Precision Measurement of the Reactor Antineutrino Spectrum with Sub-percent Energy Resolution, arXiv:2005.08745v1.
- [6] D. Renker, Geiger-mode avalanche photodiodes, history, properties and problems, NIM A 567 (2006) 48-56.
- [7] E. Garutti, Silicon photomultipliers for high energy physics detectors, JINST 6 (2011) C 10003.
- [8] VUV MPPC datasheet, <http://www.hamamatsu.com.cn>.
- [9] C. Guo, M.Y. Guan, X.L. Sun, W.X. Xiong, P. Zhang, C.G. Yang, Y.T. Wei, Y.Y. Gan, Q. Zhao, The liquid argon detector and measurement of SiPM array at liquid argon temperature, NIM A 980 (2020) 164488.
- [10] H. Yang, Z.F. Xu, J. Tang and Y. Zhang, Spin coating of TPB film on acrylic substrate and measurement of its wavelength shifting efficiency, NUCL SCI TECH 31, 28 (2020) arXiv:1911.08897.
- [11] LMH6629 datasheet, <https://www.ti.com>.
- [12] Marco D’Incecco, Cristiano Galbiati, Graham K. Giovanetti, George Korga, Xinran Li, Andrea Mandarano, Alessandro Razeto, Davide Sablone, and Claudio SavareseM, Development of a Very Low-Noise Cryogenic Preamplifier for Large-Area SiPM Devices, IEEE Transactions on Nuclear Science, vol. 65, no. 4, pp. 1005-1011, April 2018, doi: 10.1109/TNS.2018.2799325.
- [13] The DarkSide Collaboration, Cryogenic Characterization of FBK RGB-HD SiPMs, JINST 12 (2017) 9030.
- [14] An Introduction to the Silicon photomultiplier - SensL, <https://www.sensl.com>.
- [15] Patrick Eckert, Hans-Christian Schultz-Coulon, Wei Shen, Rainer Stamen, Alexander Tadday, Characterisation studies of silicon photomultipliers, NIM A 620 (2010) 217-226.
- [16] H. Fanchiotti, C.A. Garia Canal, M. Marucho, The Landua Distribution, Int. J. Mod. Phys. C 17 (2006) 1461-1476, DOI: 10.1142/S0129183106009928.

- [17] The DarkSide Collaboration, DarkSide-20k: A 20 tonne two-phase LAr TPC for direct dark matter detection at LNGS. *Eur. Phys. J. Plus* 133, 131 (2018), <https://doi.org/10.1140/epjp/i2018-11973-4>.
- [18] The DarkSide collaboration, The DarkSide project, *JINST* 11 (2016) C02051, doi:10.1088/1748-0221/11/02/C02051.
- [19] The DEAP collaboration, Constraints on dark matter-nucleon effective couplings in the presence of kinematically distinct halo substructures using the DEAP-3600 detector, *Phys. Rev. D* 102 (2020) 082001, DOI:10.1103/PhysRevD.102.082001.
- [20] W.M. Burton, B.A. Powell, Fluorescence of tetraphenyl-butadiene in the vacuum ultraviolet, *Appl. Opt.* 12 (1973) 87-89, DOI: 10.1364/AO.12.000087.
- [21] V.M. Gehman, S.R. Seibert, K. Rielage, A. Hime, Y. Sun, D.-M. Mei, J. Maassen, D. Moore, Fluorescence efficiency and visible re-emission spectrum of tetraphenyl butadiene films at extreme ultraviolet wavelengths, *NIM A* 654 (2011) 116-121.
- [22] A. Lyashenko, T. Nguyen, A. Snyder, H. Wanga and K. Arisaka, Measurement of the absolute Quantum Efficiency of Hamamatsu model R11410-10 photomultiplier tubes at low temperatures down to liquid xenon boiling point, *JINST* 9 (2014) P11021.